IUTAM Symposium on *Critical flow dynamics involving moving/deformable structures with design applications*, June 18-22, 2018, Santorini, Greece

The Dynamics of Bumblebee Wing Pitching Rotation: Measurement and Modelling

Dmitry KOLOMENSKIY[1], Sridhar RAVI[2], Ru XU[3,4], Kohei UEYAMA[3], Timothy JAKOBI[2], Thomas ENGELS[5,6], Toshiyuki NAKATA[3], Jörn SESTERHENN[6], Marie FARGE[5], Kai SCHNEIDER[7], Ryo ONISHI[1], Hao LIU[3,4]

[1] *Japan Agency for Marine-Earth Science and Technology (JAMSTEC), Japan*
[2] *School of Aerospace Mechanical and Manufacturing Engineering, RMIT University, Australia*
[3] *Graduate School of Engineering, Chiba University, Japan*
[4] *Shanghai-Jiao Tong University and Chiba University International Cooperative Research Centre (SJTU-CU ICRC), People's Republic of China*
[5] *LMD-CNRS, Ecole Normale Supérieure and PSL Paris, France*
[6] *ISTA, Technische Universität Berlin, Germany*
[7] *Institut de Mathématiques de Marseille, CNRS, Aix-Marseille Université, France*

Abstract.

Fluid-structure interaction of the flapping wings of a hovering bumblebee is considered. Kinematic reconstruction of the wing motion using synchronized high-speed video recordings is described, that provides the necessary input data for numerical modelling. Computational fluid dynamics (CFD) solver is combined with a dynamical model that describes the wing motion. Results of a numerical simulation are presented.

Key words: flapping flight, insect, bumblebee, wing, fluid-structure interaction.

1 Introduction

Many insect species are skilful hovering fliers that can generate positive lift during both upstroke and downstroke. This ability is achieved by large pitching (feathering angle) rotations of the wings necessary for maintaining positive kinematic angle of attack. Earlier research (e.g., [9, 5]) has shown that similar kinematic patterns can be produced by a wing with only up- and downstroke motion being prescribed, and elastic hinge attachment permitting passive pitching rotation. By construction, this model mimics dipteran wings, and serves a mechanism for regulating the high-frequency flapping motion only using low-frequency control input [1]. It is logical to inquire whether this control strategy can be broadly used by all flying insects. In particular, it may be suitable for hymenopterans since their hindwings are connected to the forewings by hooks. To assess the accuracy of this hypothesis, we consider hovering flight of a bumblebee *Bombus ignitus*. Our work consists of morphological measurements in order to quantify the geometrical and the inertial properties of the

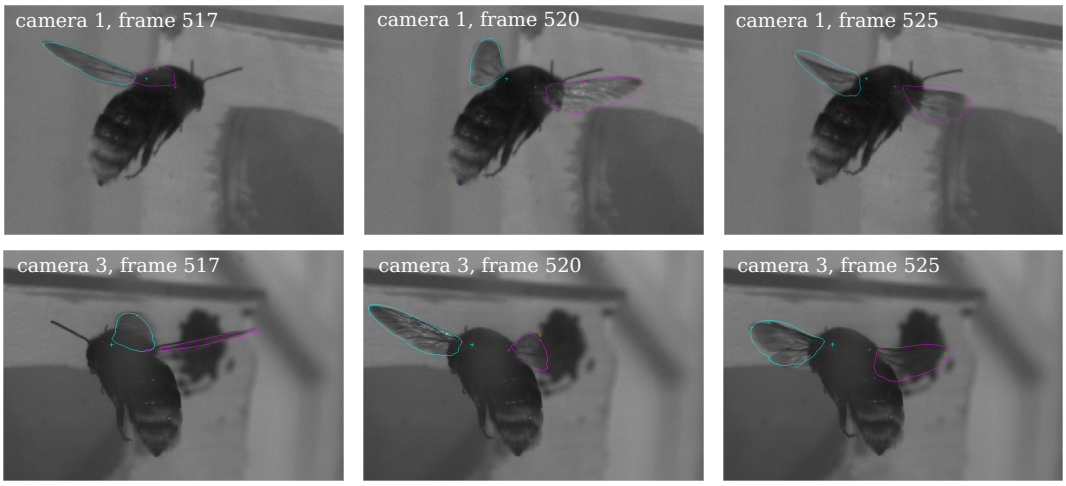

Figure 1: Sample frames from two synchronized video recordings: camera 1 (top row) and camera 3 (bottom row). Frames 517 and 520 correspond to downstroke, frames 525 correspond to upstroke. Theoretical rigid wing contour lines, shoulder points (plus signs) and body markers (dots) are superposed on the images.

wings, construction of a kinematic model of the insect, free-flight measurement of the body posture and of the wing kinematics, and computational fluid dynamics (CFD) simulations. The objective of this paper is to describe the last two steps taking one selected flight of one individual bumblebee as an example. Statistical analysis of similar results obtained for multiple individuals is our current work in progress and is will be presented elsewhere.
Section 2 describes the process of three-dimensional reconstruction of the wing kinematics from synchronized video recordings. The outcome of it is time evolution of the wing kinematic angles and the body attitude. Section 3 shows the results of a CFD numerical simulation of the same flight. Tentative conclusions are drawn in Section 4.

2 Kinematic Reconstruction

A hive (Mini Polblack, Koppert, Arysta LifeScience Asia, Japan) was maintained at Chiba University through May 2016. The bees were trained to fly through a tunnel with transparent ceiling. One end of the tunnel was connected to the hive and the other to the feeding area. In the duration of the experiment, the humidity was near to 80% and the temperature was maintained at about 22°C. The test section in the flight tunnel was illuminated using lights. The video recordings of the hovering flight discussed in this paper were acquired using three synchronized high-speed cameras (FASTCAM SA3, Photron, Japan), equipped with CCTV lens (B2514D or B5014A, Pentax, Japan) at 2000 fps, but only two views were used in the present analysis. The image resolution was set to 1024×1024 pixels. The shutter speed was $1/7500$ s. Sample frames from two cameras, with a zoom on the insect, are shown in figure 1. Extended description of the experiment and data acquisition setup can be found in [6].

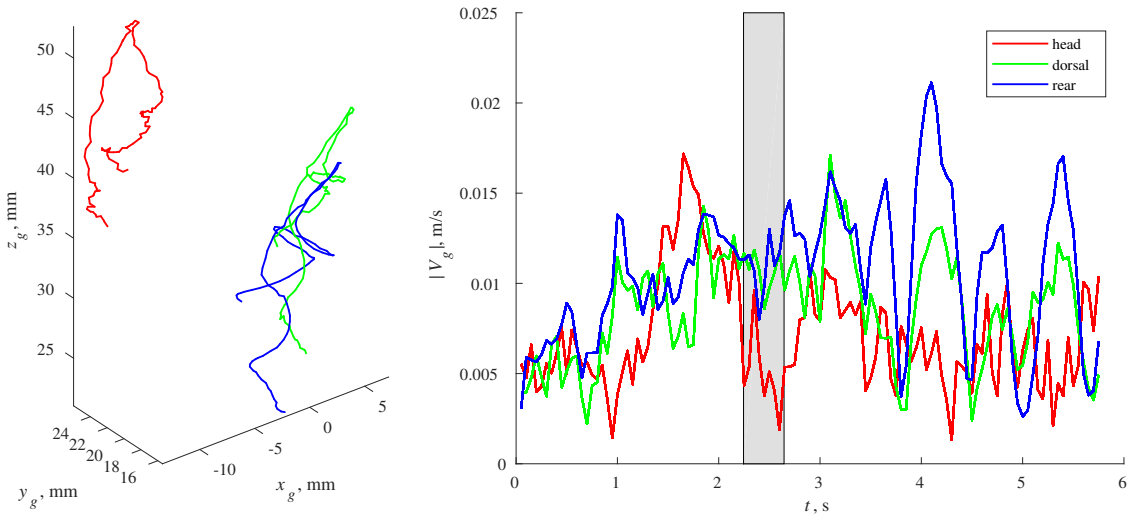

Figure 2: Left: trajectories of three points on the body - one on the head, one on the dorsal surface of the abdomen, and one on the rear end of the abdomen. Right: time evolution of the velocity magnitude of these points.

For kinematic analysis of the three-dimensional motion of the bumblebee body and flapping wings, we modified the open-source software DLTv5. The software is based on the direct linear transform method [4]. It is implemented in Matlab (MathWorks, Inc., USA). The modification mainly consists in introducing the same kinematic model as used in our CFD solver, FluSI [3]. Each forewing-hindwing pair is approximated as a single solid flat plate that can rotate about the hinge point at the shoulder, therefore its position with respect to the body is fully described with three angles. The body is also assumed rigid, therefore it is straightforward to relate the position of the shoulder points in the laboratory reference frame to the position of the center of mass and the three Euler angles of the body.

The video sequence selected for the present analysis corresponds to the hovering flight #6 in [7]. The body moves very little during the entire video. Nevertheless, this small motion should be taken into account when calculating the wing angles, because the latter are sensitive to movement of the hinges. Therefore, we first reconstructed the three-dimensional motion of the body. We selected three points that can be easily distinguished by morphological features. As shown in figure 1, point 1 is on the head between the antennae (red marker), point 2 is an abdominal pigmentation feature (green marker), and point 3 is the rear point of the abdomen (blue marker). Every 10th frame of total 1167 frames in each camera view were analyzed. The points were manually tracked and their coordinates in the laboratory reference frame reconstructed using DLTv5, the result being displayed in figure 2(left). Figure 2(right) shows the velocity magnitude of each point, calculated using central finite difference approximation. The velocity is no greater than $V_g = 0.023$ m/s, and the corresponding advance ratio is equal to $J = V_g/(2\Phi f R) = 0.0024$, where f, Φ and R are the wingbeat frequency, amplitude, and the wing length, respectively. This small advance ratio is indicative of hovering.

The time sequence of almost 6 s is longer than required for digitization of the wing motion. We therefore select only a subsequence of 40 ms for the further analy-

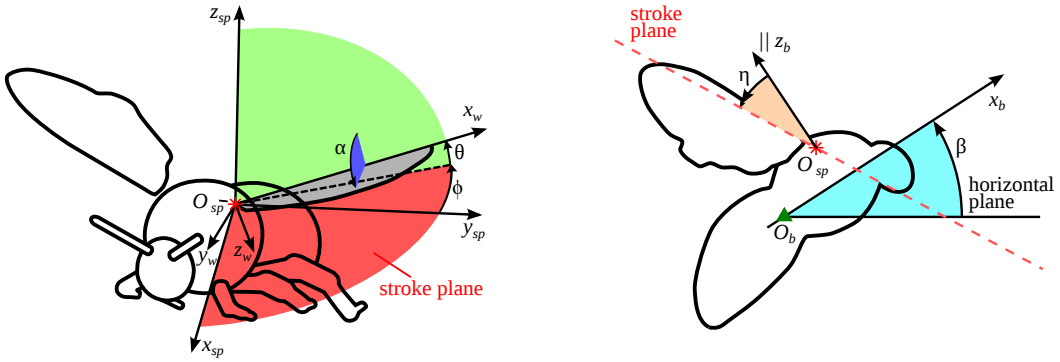

Figure 3: Definition of the wing positional angle ϕ, feathering angle α, elevation angle θ, body angle β and anatomical stroke plane angle η. O_{sp} is one of the two shoulder points, O_b is the body center of mass.

sis, which is shaded in figure 2(right). The velocity in it is less than 0.015 m/s. During this short time interval, time-varying position of the three feature points in the laboratory reference frame is fit with cubic polynomials in order to filter out the digitization noise. In the body reference frame, relative position of different points (i.e., the shoulder hinges, the center of mass and the three selected morphological features) does not vary in time, therefore, it can be determined from prior morphological measurement or time-averaging over the duration of the entire flight sequence. Hence, after reconstructing the three-dimensional motion of the selected morphological feature points, we determine the motion of the entire body including the shoulder hinge points. The latter are shown in figure 1 with cyan and magenta plus signs.

As a next step, we track the wing tips, reconstruct the wing tip trajectories, convert them to the body reference frame and best-fit a plane, in the least-mean-square sense. The morphological stroke plane angle is determined as the angle between the normal to that plane and the body longitudinal axis. The stroke plane, in our definition, is inclined at the same angle to the body and passes through the shoulder hinge points, as shown in figure 3.

Finally, we determine the time evolution of the wing angles with respect to the stroke plane, see figure 3 for the definitions. The values of the positional angle ϕ, the elevation angle θ and the feathering angle α are determined for the left and for the right wing separately, for every time frame. First approximation to ϕ and θ is calculated using the wing-tip coordinates relative to the hinge point. After that, the wing contour projection is superposed on the video image. It is drawn interactively as the values of ϕ, α and θ are manually adjusted for the best visual fit. For this purpose, as for the subsequent CFD simulation, we use the archetypal contour constructed in [8], scaled with the wing length $R = 14.6$ mm determined from the video as the average distance between the shoulder and the wing tip. Example visualizations of this fit are shown in figure 1. The digitized left (resp., right) wing contour outline is shown with a cyan (resp., magenta) closed curve. Generally, the approximation is visually better during the downstroke (first two frames in a row) than during upstroke (last frame in a row), as the wing deformation is greater during upstroke.

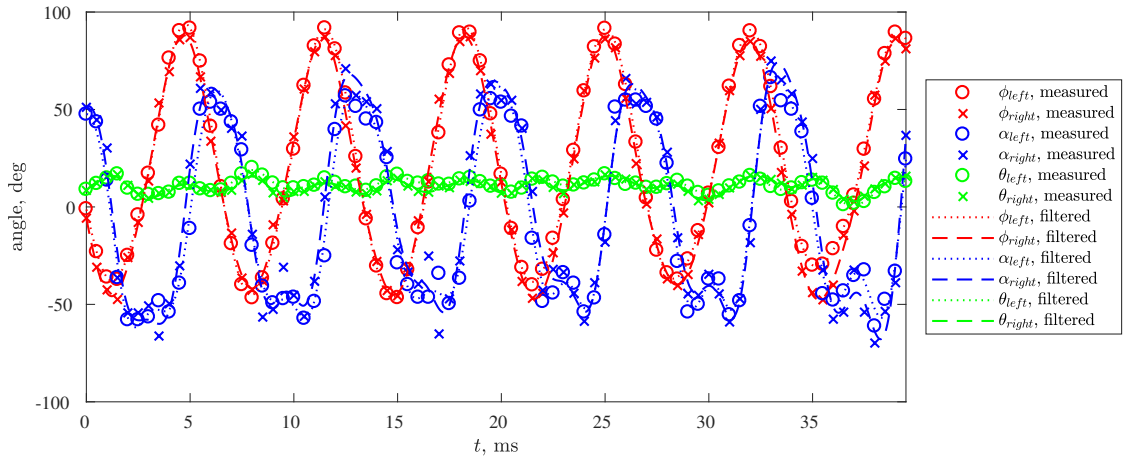

Figure 4: Time evolution of the wing kinematic angles. Markers show the raw data points obtained after digitizing each frame. Lines show the result of low-pass filtering and interpolation.

The complete measured time sequences of the wing angles are displayed as markers in figure 4. The resolution of 13 points is high enough to describe the important repetitive features of the time profiles, such as the double negative peak of α during upstroke. The motion is nominally periodic, with small deviations that may be due to actuation, fluid-structure interaction and measurement errors. The next processing step consists in low-pass filtering the data at 450 Hz using the 4th order Butterworth filter and upsampling the result on a 100-times finer grid using spline interpolation. Thus we discard those points that produce unrealistically large accelerations. The resulting time profiles are shown with dotted and dashed lines that correspond to the left and the right wing, respectively.
From frequency analysis of $\phi(t)$ we find that the flapping frequency is equal to $f = 144.6$ Hz. We use this value to divide the sequences shown in figure 4 in cycles of length $T = 1/f = 6.92$ ms. In figure 5(left), we plot the time evolution of ϕ, α and θ during each cycle, with $t = 0$ corresponding to the beginning of downstroke. The original profiles are shown with thin faded lines. For every time instant t during the cycle, we calculate the average of 4 subsequent wingbeats. The average time profiles are shown with thick bright lines in figure 5(left), and thin bright lines in figure 5(right). These time sequences are very close to periodic. There remains less than 10 degree difference between the angles of the left wing and those of the right wing, and we calculate their average. The result is plotted in figure 5(right) using thick lines. Finally, Fourier analysis of these time sequences is performed. Time evolution of ϕ, α and θ is described with less than 1 degree error using, respectively, 4, 5 and 4 harmonics. These coefficients are used as input data for the numerical simulation and analysis presented in the next section.

3 Numerical Modelling

The fluid-structure interaction model of the flapping wings has been implemented using FluSI, a pseudo-spectral Navier–Stokes solver with volume penalization [3].

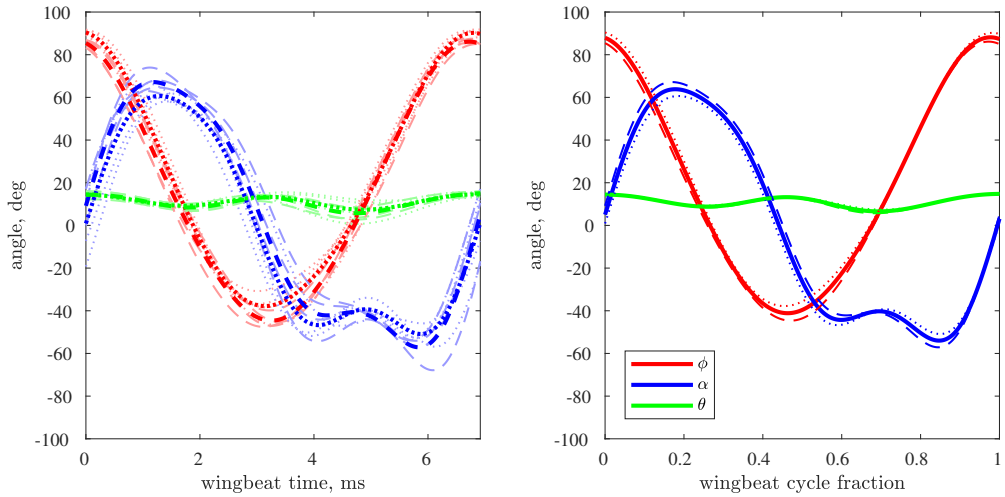

Figure 5: Left: Time evolution of the wing angles reduced to the time scale of one wingbeat (thin lines) and their average (thick lines). Right: average time profiles of the left and the right wing kinematics (thin lines) and the average of the two wings (thick lines), where the time is normalized by the wingbeat period T.

In the numerical simulation presented in this paper, the body of the bumblebee is fixed. The body shape is the same as in [2]. The shape of the wings is derived from the morphological measurements described in [8].
The positional angle $\phi(t)$ and elevation angle $\theta(t)$ of both wings are prescribed as periodic functions using Fourier coefficients, as described in the previous section. The feathering angle $\alpha(t)$ is determined from the following driven oscillator equation [9]:

$$\begin{aligned} I_{yy}\ddot{\alpha} = {} & M_{aero} - K(\alpha - \alpha_0) - C\dot{\alpha} \\ & + I_{yy}\left[\frac{1}{2}(\dot{\phi}^2\cos^2\theta - \dot{\theta}^2)\sin 2\alpha - \ddot{\phi}\sin\theta - \dot{\phi}\dot{\theta}\cos\theta(1+\cos 2\alpha)\right] \\ & + I_{xy}\left[\ddot{\phi}\cos\theta\cos\alpha + \ddot{\theta}\sin\alpha + \frac{1}{2}\dot{\phi}^2\sin 2\theta\sin\alpha - 2\dot{\phi}\dot{\theta}\sin\theta\cos\alpha\right], \end{aligned} \quad (1)$$

where M_{aero} is the aerodynamic pitching moment. Positive θ is upwards. Typically, α is positive during downstroke and negative during upstroke. The moments of inertia are determined by integration of mass distribution in the $x_w - y_w$ plane of the wing, assuming that it is thin and flat, as follows:

$$I_{yy} = \int_{\Sigma_w} x_w^2 \mathrm{d}m_w, \qquad I_{xy} = \int_{\Sigma_w} x_w y_w \mathrm{d}m_w, \quad (2)$$

where Σ_w is the wing surface, $\mathrm{d}m_w$ is the planar mass element of the wing, and (x_w, y_w) are the coordinates of the element, see [8] for more detail. The aerodynamic pitching moment M_{aero} is obtained by integrating the fluid forces acting on the wing. The shoulder hinge joint is modelled as a torsional spring with stiffness K, damping coefficient C and neutral angle α_0.
An example result of the numerical simulation is shown in figure 6. The parameters of the numerical simulation are as follows. The wing length is equal to $R = 14.6$ mm

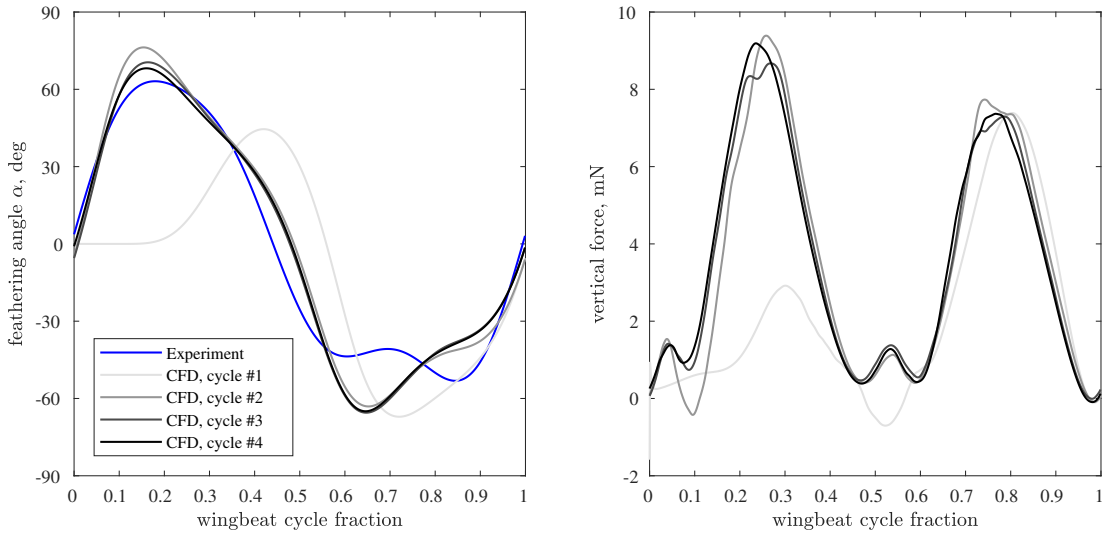

Figure 6: Left: time evolution of the feathering angle in the experiments and i the numerical simulation. Right: time evolution of the instantaneous aerodynamic vertical force.

and the flapping frequency is $f = 144.6$ Hz, as described in the previous section. The wing beat amplitude that follows from figure 5(right) is $\Phi = 129$ deg. Using the notation as in figure 3, the body angle is equal to $\beta = 47.8$ deg and the anatomical stroke plane angle is $\eta = 41$ deg. The elastic hinge model uses the stiffness $K = 2.52 \times 10^{-6}$ N m, damping $C = 0$ and neutral angle $\alpha_0 = -0.7$ deg. The wing moments of inertia are equal to $I_{yy} = 28.14 \times 10^{-12}$ kg m^2 and $I_{xy} = -0.70 \times 10^{-12}$ kg m^2.

Since the flapping motion started impulsively at the beginning of the numerical simulation, to avoid excessively large values of M_{aero} at startup, the right-hand side of (1) was multiplied with a function smoothly varying from 0 to 1 during the time interval from 0.1 to 0.5 of the wingbeat period T. Therefore, the results of the simulation during the first wingbeat cycle are not physically significant. To reach quasi-periodic state of $\alpha(t)$ and the aerodynamic forces, the time span of the numerical simulation was set to $4T$.

In figure 6, gradations of grey are used to distinguish between the results that correspond to different wingbeat cycles in the numerical simulation. Time variation of α is almost the same during the last two cycles, see figure 6(right). The r.m.s. distance is less than 11 deg with respect to $\alpha(t)$ obtained from the measurement described in the previous section (the blue line in figure 6). This value is of the same order of magnitude as the combined error of digitization, periodization, etc. The most obvious discrepancy is in the middle of upstroke when the model neglects wing deformation and, in particular, rotation of the hindwing relatively to the forewing. A more sophisticated deformable wing model may be necessary to reach better agreement in terms of $\alpha(t)$. Nonetheless, the agreement is reasonably good even using the present single-plate model, therefore, it is not surprising that the time-varying vertical force obtained from the model (figure 6 right) displays the double peak profile typical of hovering insects. The mean vertical force is large enough to support the body mass of 364 mg that is realistic for a bumblebee of this size.

4 Conclusions

In this paper, we discussed about application of a hinged-plate model to analyze pitching motion of flapping wings of a bumblebee during hovering. We described the methodology of kinematic reconstruction based on synchronized video recordings and presented an example of aerodynamic force calculation using CFD. In the model, the forewing and the hindwing are approximated by a one-piece rigid flat plate. Analysis of the video recordings suggests that the rigid wing contour can be adequately fit with outline of the real wing, despite some deformation of the latter. Numerical solution of the differential equation that governs the dynamics of the model, integrated with a Navier–Stokes solver, results in the wing pitching motion similar to that observed in the experiment. The r.m.s. error is less that 11 deg, and the discrepancy is essentially localized around the middle upstroke, when the flat wing approximation may fail. Nevertheless, the model successfully predicts the time evolution of the lift force with two almost equal peaks, one during downstroke and the other during upstroke, that is typical of hovering insets wings. The mean vertical aerodynamic force estimated from the numerical simulation is reasonably large to support the body weight.

Acknowledgements

DK gratefully acknowledges financial support from the JSPS Grant-in-Aid 18K13693. TE, JS, MF, KS gratefully acknowledge financial support from the Agence nationale de la recherche (ANR Grant 15-CE40-0019) and Deutsche Forschungsgemeinschaft (DFG Grant SE 824/26-1), project AIFIT.

References

[1] T. Beatus and I. Cohen. Wing-pitch modulation in maneuvering fruit flies is explained by an interplay between aerodynamics and a torsional spring. *Physical Review E*, 92(2):022712, 2015.

[2] T. Engels, D. Kolomenskiy, K. Schneider, F.-O. Lehmann, and J. Sesterhenn. Bumblebee flight in heavy turbulence. *Physical Review Letters*, 116(2):028103, 2016.

[3] T. Engels, D. Kolomenskiy, K. Schneider, and J. Sesterhenn. A novel parallel simulation tool for flapping insect flight using a Fourier method with volume penalization. *SIAM Journal on Scientific Computing*, 38(5):S3–S24, 2016.

[4] T. L. Hedrick. Software techniques for two- and three-dimensional kinematic measurements of biological and biomimetic systems. *Bioinspiration & Biomimetics*, 3(3):034001, 2008.

[5] D. Ishihara, T. Horie, and T. Niho. An experimental and three-dimensional computational study on the aerodynamic contribution to the passive pitching motion of flapping wings in hovering flies. *SIAM Journal on Scientific Computing*, 9(4):046009, 2014.

[6] T. Jakobi, D. Kolomenskiy, T. Ikeda, S. Watkins, A. Fisher, H. Liu, and S. Ravi. Bees with attitude: the effect of gusts on flight dynamics. *arXiv*, 1802.03580, 2018.

[7] D. Kolomenskiy, S. Ravi, K. Ueyama, T. Jakobi, R. Xu, H. Liu, R. Onishi, T. Engels, K. Schneider, J. Sesterhenn, and M. Farge. Bumblebee flight kinematics, Jan 2018. Dataset retrieved from: osf.io/2fked, last accessed on May 16, 2018.

[8] D. Kolomenskiy, S. Ravi, R. Xu, K. Ueyama, T. Jakobi, T. Engels, T. Nakata, J. Sesterhenn, M. Farge, K. Schneider, R. Onishi, and H. Liu. The dynamics of bumblebee wing pitching

rotation: wing morphology and inertial properties. In *Proceedings of the 7th International Symposium on Aero Aqua Bio-mechanisms*. ABMECH.

[9] J. P. Whitney and R. J. Wood. Aeromechanics of passive rotation in flapping flight. *Journal of Fluid Mechanics*, 660:197–220, 2010.